A&A 577, A131 (2015)
DOI: 10.1051/0004-6361/201525699

Astronomy & Astrophysics

Discovery of variable VHE γ-ray emission from the binary system 1FGL J1018.6–5856

H.E.S.S. Collaboration, A. Abramowski[1], F. Aharonian[2,3,4], F. Ait Benkhali[2], A. G. Akhperjanian[5,4], E. O. Angüner[6], M. Backes[7], A. Balzer[8], Y. Becherini[9], J. Becker Tjus[10], D. Berge[11], S. Bernhard[12], K. Bernlöhr[2], E. Birsin[6], R. Blackwell[13], M. Böttcher[14], C. Boisson[15], J. Bolmont[16], P. Bordas[2], J. Bregeon[17], F. Brun[18], P. Brun[18], M. Bryan[8], T. Bulik[19], J. Carr[20], S. Casanova[21,2], N. Chakraborty[2], R. Chalme-Calvet[16], R. C. G. Chaves[17,22], A. Chen[23], M. Chrétien[16], S. Colafrancesco[23], G. Cologna[24], J. Conrad[25,⋆], C. Couturier[16], Y. Cui[26], I. D. Davids[14,7], B. Degrange[27], C. Deil[2], P. deWilt[13], A. Djannati-Ataï[28], W. Domainko[2], A. Donath[2], L. O'C. Drury[3], G. Dubus[29], K. Dutson[30], J. Dyks[31], M. Dyrda[21], T. Edwards[2], K. Egberts[32], P. Eger[2], J.-P. Ernenwein[20], P. Espigat[28], C. Farnier[25], S. Fegan[27], F. Feinstein[17], M. V. Fernandes[1], D. Fernandez[17], A. Fiasson[33], G. Fontaine[27], A. Förster[2], M. Füßling[34], S. Gabici[28], M. Gajdus[6], Y. A. Gallant[17], T. Garrigoux[16], G. Giavitto[34], B. Giebels[27], J. F. Glicenstein[18], D. Gottschall[26], A. Goyal[35], M.-H. Grondin[36], M. Grudzińska[19], D. Hadasch[12], S. Häffner[37], J. Hahn[2], J. Hawkes[13], G. Heinzelmann[1], G. Henri[29], G. Hermann[2], O. Hervet[15], A. Hillert[2], J. A. Hinton[2,30], W. Hofmann[2], P. Hofverberg[2], C. Hoischen[32], M. Holler[27], D. Horns[1], A. Ivascenko[14], A. Jacholkowska[16], C. Jahn[37], M. Jamrozy[35], M. Janiak[31], F. Jankowsky[24], I. Jung-Richardt[37], M. A. Kastendieck[1], K. Katarzyński[38], U. Katz[37], D. Kerszberg[16], B. Khélifi[28], M. Kieffer[16], S. Klepser[34], D. Klochkov[26], W. Kluźniak[31], D. Kolitzus[12], Nu. Komin[23], K. Kosack[18], S. Krakau[10], F. Krayzel[33], P. P. Krüger[14], H. Laffon[36], G. Lamanna[33], J. Lau[13], J. Lefaucheur[28], V. Lefranc[18], A. Lemière[28], M. Lemoine-Goumard[36], J.-P. Lenain[16], T. Lohse[6], A. Lopatin[37], C.-C. Lu[2], R. Lui[2], V. Marandon[2], A. Marcowith[17], C. Mariaud[27], R. Marx[2], G. Maurin[33], N. Maxted[17], M. Mayer[6], P. J. Meintjes[39], U. Menzler[10], M. Meyer[25], A. M. W. Mitchell[2], R. Moderski[31], M. Mohamed[24], K. Morå[25], E. Moulin[18], T. Murach[6], M. de Naurois[27], J. Niemiec[21], L. Oakes[6], H. Odaka[2], S. Öttl[12], S. Ohm[34], E. de Oña Wilhelmi[2,42,⋆⋆], B. Opitz[1], M. Ostrowski[35], I. Oya[34], M. Panter[2], R. D. Parsons[2], M. Paz Arribas[6], N. W. Pekeur[14], G. Pelletier[29], P.-O. Petrucci[29], B. Peyaud[18], S. Pita[28], H. Poon[2], H. Prokoph[9], G. Pühlhofer[26], M. Punch[28], A. Quirrenbach[24], S. Raab[37], I. Reichardt[28], A. Reimer[12], O. Reimer[12], M. Renaud[17], R. de los Reyes[2], F. Rieger[2,40], C. Romoli[3], S. Rosier-Lees[33], G. Rowell[13], B. Rudak[31], C. B. Rulten[15], V. Sahakian[5,4], D. Salek[41], D. A. Sanchez[33], A. Santangelo[26], M. Sasaki[26], R. Schlickeiser[10], F. Schüssler[18], A. Schulz[34], U. Schwanke[6], S. Schwemmer[24], A. S. Seyffert[14], R. Simoni[8], H. Sol[15], F. Spanier[14], G. Spengler[25], F. Spies[1], Ł. Stawarz[35], R. Steenkamp[7], C. Stegmann[32,34], F. Stinzing[37], K. Stycz[34], I. Sushch[14], J.-P. Tavernet[16], T. Tavernier[28], A. M. Taylor[3], R. Terrier[28], M. Tluczykont[1], C. Trichard[33], K. Valerius[37], J. van der Walt[14], C. van Eldik[37], B. van Soelen[39], G. Vasileiadis[17], J. Veh[37], C. Venter[14], A. Viana[2], P. Vincent[16], J. Vink[8], F. Voisin[13], H. J. Völk[2], T. Vuillaume[29], S. J. Wagner[24], P. Wagner[6], R. M. Wagner[25], M. Weidinger[10], Q. Weitzel[2], R. White[30], A. Wierzcholska[24,21], P. Willmann[37], A. Wörnlein[37], D. Wouters[18], R. Yang[2], V. Zabalza[30,⋆⋆], D. Zaborov[27], M. Zacharias[24], A. A. Zdziarski[31], A. Zech[15], F. Zefi[27], and N. Żywucka[35]

(Affiliations can be found after the references)

Received 20 January 2015 / Accepted 9 March 2015

ABSTRACT

Re-observations with the HESS telescope array of the very high-energy (VHE) source HESS J1018–589 A that is coincident with the *Fermi*-LAT γ-ray binary 1FGL J1018.6–5856 have resulted in a source detection significance of more than 9σ and the detection of variability (χ^2/ν of 238.3/155) in the emitted γ-ray flux. This variability confirms the association of HESS J1018–589 A with the high-energy γ-ray binary detected by *Fermi*-LAT and also confirms the point-like source as a new VHE binary system. The spectrum of HESS J1018–589 A is best fit with a power-law function with photon index $\Gamma = 2.20 \pm 0.14_{\rm stat} \pm 0.2_{\rm sys}$. Emission is detected up to ~20 TeV. The mean differential flux level is $(2.9 \pm 0.4) \times 10^{-13}$ TeV^{-1} cm^{-2} s^{-1} at 1 TeV, equivalent to ~1% of the flux from the Crab Nebula at the same energy. Variability is clearly detected in the night-by-night light curve. When folded on the orbital period of 16.58 days, the rebinned light curve peaks in phase with the observed X-ray and high-energy phaseograms. The fit of the HESS phaseogram to a constant flux provides evidence of periodicity at the level of $N_\sigma > 3\sigma$. The shape of the VHE phaseogram and measured spectrum suggest a low-inclination, low-eccentricity system with a modest impact from VHE γ-ray absorption due to pair production ($\tau \lesssim 1$ at 300 GeV).

Key words. gamma rays: stars – stars: individual: 1FGL J1018.6-5856 – radiation mechanisms: non-thermal – acceleration of particles – X-rays: binaries

⋆ Wallenberg Academy Fellow.

⋆⋆ Corresponding authors: E. de Oña Wilhelmi, e-mail: emma@mpi-hd.mpg.de; V. Zabalza, e-mail: victor.zabalza@le.ac.uk

1. Introduction

The region around the supernova remnant SNR G284.3–1.8 (Milne et al. 1989) shows two clearly distinct regions of very high-energy (VHE; $E > 100$ GeV) γ-ray emission (Abramowski et al. 2012); an extended emission named HESS J1018–589 B probably associated with the pulsar wind nebula (PWN) powered by the bright pulsar PSR J1016–5857 (Camilo et al. 2001, 2004), and the point-like source HESS J1018–589 A. The latter is positionally coincident with 1FGL J1018.6–5856, a point-like high-energy γ-ray (HE; 100 MeV $< E <$ 100 GeV) variable source detected by the *Fermi* Large Area Telescope (LAT; Abdo et al. 2010).

The γ-ray binary 1FGL J1018.6–5856 was detected in a blind search for periodic sources in the *Fermi*-LAT survey of the Galactic Plane through the modulation of its HE γ-ray flux (Ackermann et al. 2012). Optical observations show that the non-thermal source is positionally coincident with a massive star of spectral type O6V((f)). The radio and X-ray flux from the source are modulated with the same period of 16.58±0.02 days, which is interpreted as the binary orbital period (Pavlov et al. 2011; Li et al. 2011; Abramowski et al. 2012; An et al. 2013).

The spectrum of the periodic source in the *Fermi*-LAT domain exhibits a break at ∼1 GeV with best-fit values of $\Gamma_{\rm HE}$(0.1–1 GeV) = 2.00 ± 0.04 and $\Gamma_{\rm HE}$(1–10 GeV) = 3.09 ± 0.06 and an integral energy flux above 100 MeV of (2.8 ± 0.1) × 10^{-10} erg cm^{-2} s^{-1}. The HE γ-ray spectral shape evolves with orbital phase, with a decrease in spectral curvature at flux minimum of the emission (between phases 0.2 and 0.6) and a hardening of the spectrum at flux maximum.

The best-fit position reported in the previous paper (Abramowski et al. 2012) for HESS J1018–589 A, $\alpha = 10^{\rm h}18^{\rm m}59.3^{\rm s} \pm 2.4^{\rm s}_{\rm stat}$ and $\delta = -58°56'10'' \pm 36''_{\rm stat}$ (J2000), is compatible with the 95% confidence contour of 1FGL J1018.6–5856. The VHE emission is well-described by a power-law function with a spectral index of $\Gamma = 2.7 \pm 0.5_{\rm stat} \pm 0.2_{\rm sys}$, similar to the one describing the VHE emission of the larger region HESS J1018–589 B ($\Gamma = 2.9 \pm 0.4_{\rm stat} \pm 0.2_{\rm sys}$). No variability was found in the HESS data set, although the contamination of the nearby source and the uneven sampling of the observations prevented a firm conclusion at the time.

Here, a deeper study of HESS J1018–589 A to assess its association with the γ-ray binary is presented. In Sect. 2, the data sample and results are described. In Sect. 3, the features of HESS J1018–589 A are discussed in light of the multi-wavelength observations available, and conclusions are drawn in Sect. 4.

2. Data analysis and results

The HESS telescope array is a system of five VHE γ-ray imaging atmospheric Cherenkov telescopes (IACTs) located in the Khomas Highland of Namibia (23°16′18″ S, 16°30′00″ E). The fifth telescope was added to the array in summer 2012 during the HESS phase-II upgrade, increasing the energy coverage and boosting the system sensitivity. The nominal sensitivity of the HESS phase-I array (excluding the large telescope) reached in 25 h is ∼2.0×10^{-13} ph cm^{-2} s^{-1} (equivalent to 1% of the Crab Nebula flux above 1 TeV) for a point-like source detected at a significance of 5σ at zenith. The stereoscopic approach results in a positional reconstruction uncertainty of ∼6′ per event, good energy resolution (15% on average), and an efficient background rejection (Aharonian et al. 2006). HESS-I observed the region towards the Carina arm from 2004 to 2009. The data set

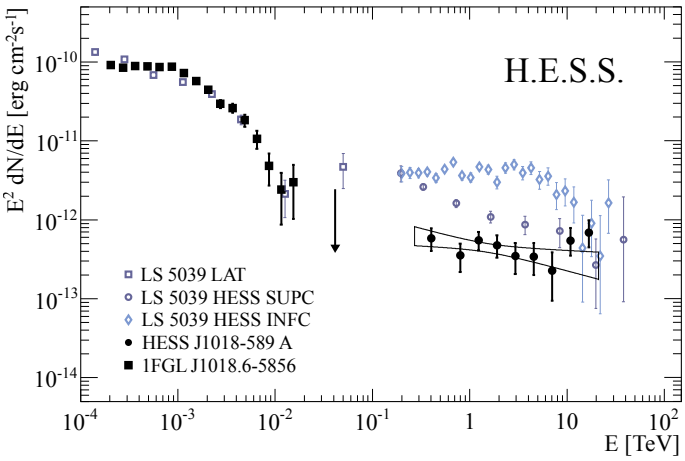

Fig. 1. SED of HESS J1018–589 A/1FGL J1018.6–5856 is shown in black (filled squares and circles for the LAT and HESS detection). For comparison, the SEDs of LS 5039 during superior (SUPC) and inferior conjunction (INFC) are also included (blue points from Hadasch et al. 2012; Aharonian et al. 2005a).

presented in Abramowski et al. (2012) was increased in the subsequent years from 40 h to 63.3 h effective time with dedicated observations with the HESS-I array to cover the orbital phases in which the emission of 1FGL J1018.6–5856 observed in X-rays and HE increases. The zenith angle at which the source was observed ranged from 35° to 55°, resulting in a mean energy threshold of 0.35 TeV. These new observations were performed in wobble-mode, during which the telescopes were pointed offset (0.7°) from the nominal source location to allow simultaneous background estimation. The data were analysed using an improved analysis technique (multivariate analysis, reaching ∼0.7% of the Crab Nebula flux at 1 TeV, 5σ; Becherini et al. 2011) and were cross-checked with the Hillas second-moment event reconstruction method (Aharonian et al. 2006) and a semi-analytical model analysis (de Naurois & Rolland 2009), including independent calibration of pixel amplitudes and identification of problematic or dead pixels in the IACTs cameras. The spectra and light curves shown here are derived for a cut of 80 photoelectrons in the intensity of the recorded images.

The new analysis of HESS J1018–589 A, using the larger data set, confirms the point-like VHE γ-ray emission reported in Abramowski et al. (2012). The γ-ray signal is detected with a statistical significance of 9.3σ pre-trials (derived using an oversampling radius of 0.10° and corresponding to more than 7.5σ post-trials), centred at $\alpha = 10^{\rm h}18^{\rm m}58^{\rm s} \pm 5^{\rm s}_{\rm stat}$ and $\delta = -58°56'43'' \pm 30''_{\rm stat}$ (J2000). The best-fit position is estimated by means of a maximum-likelihood fit of the exposure-corrected uncorrelated excess image. This position is compatible with the position derived in Abramowski et al. (2012), but the nearby extended source HESS J1018–589 B precludes an improvement in the position uncertainty even with the additional observation time. The fitted extension is compatible with the HESS point spread function (PSF, estimated to have a mean 68% containment radius of ∼0.1°). The obtained position is used to derive the spectrum of the point-like source, integrating in a circle of 0.1° around it and using a forward-folding maximum-likelihood fit (Piron et al. 2001). The photon spectrum is well-described with a power-law function with index $\Gamma = 2.20 \pm 0.14_{\rm stat} \pm 0.2_{\rm sys}$ (Fig. 1), and the flux normalisation is $N_0 = (2.9 \pm 0.4_{\rm stat}) \times 10^{-13}$ TeV^{-1} cm^{-2} s^{-1} at 1 TeV. The

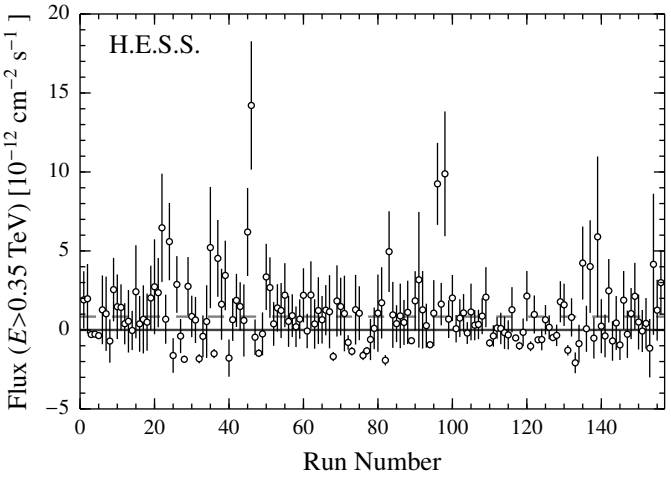

Fig. 2. Light curve of the integral flux above 0.35 TeV in a 0.1° region centred on HESS J1018–589 A binned by observation run, corresponding to approximately 30 min of observation time per bin. The dashed horizontal line shows the mean integral flux.

systematic error on the normalisation constant N_0 is estimated to be 20% (Aharonian et al. 2006). The better statistics allow for a better determination of the spectral features of the point-like source compared with the one presented in Abramowski et al. (2012), including a clearer separation from HESS J1018–589 B. The nearby source introduces a maximum of 30% contamination on HESS J1018–589 A, although above 1 TeV, thanks to the better PSF, a contamination lower than 10% was calculated from a simultaneous fit of the two sources.

The light curve of the source above 0.35 TeV, binned by observation run (approximately 30 min of observation time), is shown in Fig. 2. The best-fit mean flux level above 0.35 TeV is marked with a dashed grey line. The light curve displays clear variability, with a χ^2/ν of 238.3/155 (corresponding to 4.3σ) using a likelihood-ratio test with a constant flux as null hypothesis.

To investigate the periodicity of the source, the data were folded with the 16.58-day period found in the HE γ-ray observations (Fig. 3, top panel) using the reference time of $T_{\rm max}$ = 55 403.3 MJD as phase 0 (Ackermann et al. 2012) in a single trial. The number of bins in the phaseogram was selected to obtain a significance of at least 1σ in each phase bin. For comparison, the same phaseogram is also shown for HESS J1023–589, a nearby bright γ-ray source expected to be constant. The flux variation along the orbit shows a similar behaviour as the *Fermi*-LAT flux integrated between 1 and 10 GeV (Fig. 3, middle-top panel). An increase of the flux towards phase 0 is observed, with a χ^2/ν of 22.7/7 (3.1σ) when fitting the histogram to a constant flux, providing evidence of periodicity at the a priori selected period. Unfortunately, the uneven sampling and long timespan of the observations did not allow for an independent determination of the periodicity from the VHE γ-ray data using a Lomb-Scargle test (Scargle 1982), since the equivalent frequency is about eight times higher than the sample Nyquist frequency. Finally spectral modulation was examined by deriving the photon spectrum for observations in the 0.2 to 0.6 phase range (motivated by the *Fermi*-LAT observations) and comparing it with the one derived at the maximum of the emission in the complementary phase range. No spectral modulation was found within the photon index errors ($\Delta\Gamma$ = 0.36 ± 0.43), although it should be noted that the data statistics in the 0.2 to 0.6 phase range are

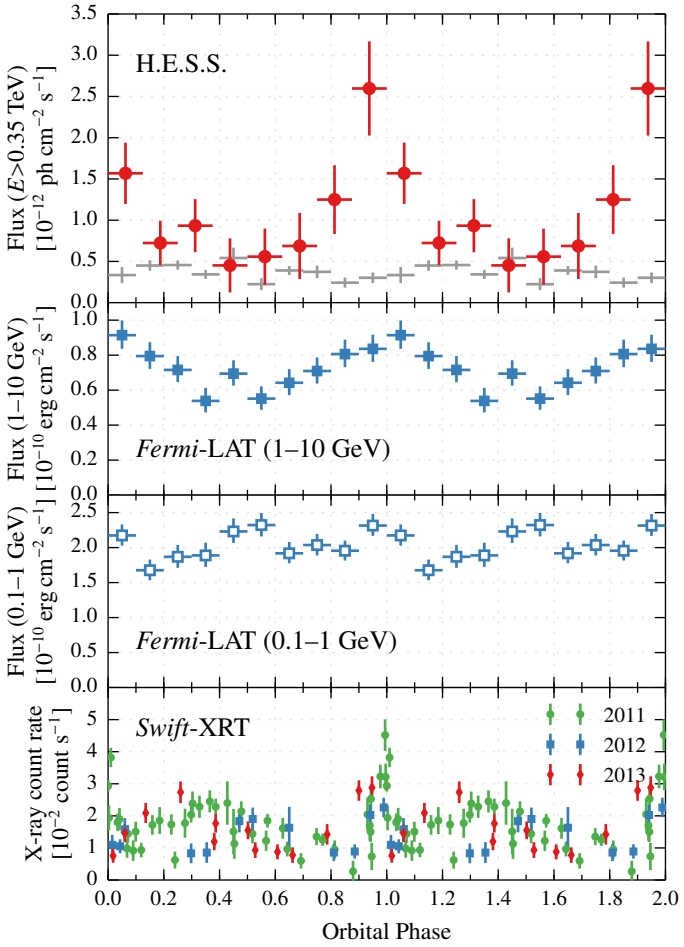

Fig. 3. VHE, HE, and X-ray fluxes of 1FGL J1018.6–5856 folded with the orbital period of P = 16.58 d. Two orbits are shown for clarity. *Top*: VHE integral flux above 0.35 TeV measure by HESS (red circles). For comparison, a scaled light curve from the nearby bright source HESS J1023-589 is shown in grey. *Middle top and middle bottom*: *Fermi*-LAT light curve between 1 and 10 GeV (solid blue squares) and between 0.1 and 1 GeV (open blue squares; Ackermann et al. 2012). *Bottom*: X-ray 0.3–10 keV count-rate light curve from 67 *Swift*-XRT observations in 2011 (green), 2012 (blue), and 2013 (red).

insufficient (3σ detection) to firmly conclude a lack of variation in the spectrum at different orbital phases.

To compare the VHE orbital modulation with the behaviour of the source at X-ray energies, we analysed 67 *Swift*-XRT observations of 1FGL J1018.6–5856, performed between 2011 and 2013 and with a median observation time of 2.2 ksec. Early subsets of these observations were presented previously by Ackermann et al. (2012) and An et al. (2013). Cleaned event files were obtained using `xrtpipeline` from HEAasoft v6.15.1. For each observation, source count rates were extracted from a circular region of 1 arcmin around the nominal position of 1FGL J1018.6–5856, and background count rates extracted from a nearby region of the same size devoid of sources. The resulting count-rate light curve, folded with the orbital period, is shown in the bottom panel of Fig. 3. The phaseogram displays a sharp peak around phase 0, matching the location of the maximum in the VHE and HE phaseograms. There is an additional sinusoidal component with a maximum around phase 0.3 and with lower amplitude than the sharp peak at phase 0.

3. Discussion

The flux variability and periodical behaviour of HESS J1018–589 A suggest the identification of the VHE source with the γ-ray binary 1FGL J1018.6–5856. It therefore becomes the fifth binary system, along with LS 5039 (Aharonian et al. 2005a), LS I +61 303 (Albert et al. 2006), PSR B1259–63 (Aharonian et al. 2005b), and HESS J0632+057 (Acciari et al. 2009), that is detected at VHE during multiple orbits, in addition to the hint of a flaring episode from the X-ray binary Cygnus X-1 (Albert et al. 2007). When folded with the modulation period found at other wavelengths, the rebinned VHE light curve shows a modulation, significant at the 3.1σ level, in phase with the HE γ-ray light curve. The phaseogram (Fig. 3) shows a similar behaviour (within the limited statistics) to the high-energy light curve of 1FGL J1018.6–5856 showing a flux increasing simultaneously to the one occurring in the HE and X-ray counterpart.

Despite the different orbital behaviour at different wavelengths, the stars in the γ-ray binaries 1FGL J1018.6–5856 and LS 5039 are thought to be very similar, with spectral types of O6V((f)) and O6.5V((f)), respectively (Ackermann et al. 2012; Clark et al. 2001). Unfortunately, the orbital parameters of HESS J1018–589 A are not yet known, and only limited conclusions can be drawn on the relation between the compact object and the massive star. Both binary systems are composed of an almost identical massive star and a compact object orbiting it on a timescale of days. The period of 1FGL J1018.6–5856 is four times longer, which implies a semi-major axis larger by a factor ~2.5 than in LS 5039, and the low amplitude of the flux modulation observed by *Fermi*-LAT, of about 25%, can be interpreted as a sign of a low-eccentricity orbit. Although the spectral-index variability at HE γ-ray is at odds with anisotropic IC being the only source of flux variability, such a low modulation amplitude would be difficult to realize under the widely changing conditions of an eccentric orbit. The behaviour of HESS J1018–589 A at different orbital phases is mimicked in X-rays, HE, and VHE, showing in all cases a maximum flux near phase 0. There is a second sinusoidal component that peaks at phase 0.3 and appears in radio (Ackermann et al. 2012) and X-rays (Fig. 3, bottom panel), as well as a hint in the 0.1 to 1 GeV *Fermi*-LAT light curve peaking at phase 0.5 (Fig. 3, middle-bottom panel), but it is not observed (with the current statistics) at higher energies. However, in LS 5039 the VHE flux is correlated with the X-ray flux, but anti-correlated with the HE flux (Aharonian et al. 2005a; Takahashi et al. 2009; Hoffmann et al. 2009; Hadasch et al. 2012). The HE spectral energy distributions (SEDs) of the two binary systems are remarkably similar in shape and flux (see Fig. 1), although it should be noted that the systems are believed to be located at different distances: whereas LS 5039 is ~2.5 kpc away, 1FGL J1018.6–5856 is believed to be located at 5 ± 2 kpc. This distance is derived from the interstellar absorption lines of the companion (Ackermann et al. 2012). At VHE, LS 5039 shows a clear spectral modulation at different orbital phases, with a mean luminosity between 1 and 10 TeV of $\sim 10^{33} (d_{2.5\,\mathrm{kpc}})^2\,\mathrm{erg\,s^{-1}}$, similar to the one found in HESS J1018–589 A in the same energy range ($9.9 \times 10^{32} (d_{5\,\mathrm{kpc}})^2\,\mathrm{erg\,s^{-1}}$). However, the ratios between the fluxes measured at HE and VHE of the two binary systems differ substantially (see Figs. 1 and 3): whereas for LS 5039 the ratio between the fluxes at 1 GeV and 1 TeV varies between ~15 and 40 in superior and inferior conjunction, respectively, for 1FGL J1018.6–5856 and HESS J1018–589 A a ratio of ~160 is found, with the TeV flux strongly reduced with respect to the GeV flux when compared with LS 5039. Similar to other binaries, the spectrum of 1FGL J1018.6–5856 measured at HE does not extrapolate to VHE.

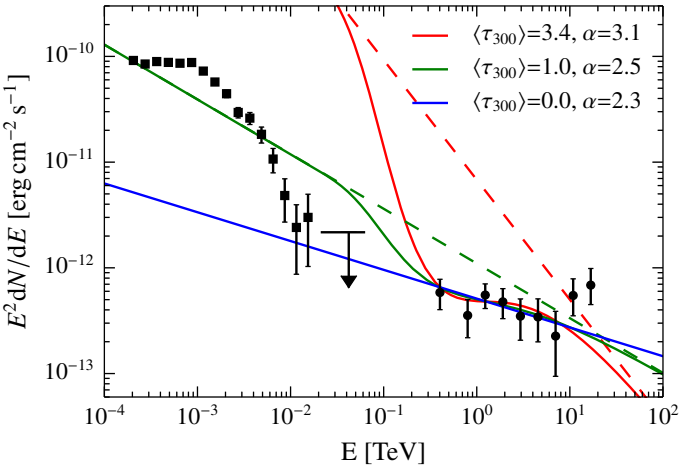

Fig. 4. Results of the fit of a pair-production-absorbed power-law to the HE and VHE spectra of 1FGL J1018.6–5856, with solid (dashed) lines indicating the absorbed (intrinsic) spectra. The emitter is assumed to be in the plane of the sky with respect to the star (i.e., on the plane of an orbit with $i = 0°$). The model with the maximum absorption compatible with the VHE spectral data is shown in red, the best-fit model with $\langle\tau_{300}\rangle = 1$ in green, and the best-fit model with no absorption in blue. Observational points are the same as in Fig. 1.

Regardless of the nature of the emission process responsible for the TeV emission, the strong stellar photon field in the environment of the binary system unavoidably leads to the absorption of γ-rays above ~50 GeV through pair production (Moskalenko & Karakula 1994; Böttcher & Dermer 2005; Dubus 2006). Assuming that the VHE emission is due to anisotropic inverse-Compton (IC) scattering of a leptonic population at a similar location as the HE emission, the identical phasing of HE and VHE would imply a low inclination of the orbit with respect to the observing direction. Furthermore, the sinusoidal modulation implies that the orbit cannot be highly eccentric (or the density of photons would lead to strong variation). Assuming this scenario, IC anisotropic emission would be most efficient when the emitter is behind the star with respect to the emitter, that is, at superior conjunction, and therefore the flux maximum at phase 0 can be tentatively associated with this orbital configuration.

To illustrate the effects of absorption on the observed VHE spectrum, in the following calculations a circular orbit on the plane of the sky ($i = 0°$) is assumed to exemplify the low, but probably non-zero, inclination of the orbit, and take stellar parameters as in LS 5039. A fit of a pair-production-absorbed power-law function (of shape $\propto E^{-\alpha} \exp(-\langle\tau_E\rangle)$, where $\langle\tau_E\rangle$ is the energy-dependent orbit-averaged optical depth and α the intrinsic spectral index) to the measured VHE spectrum indicates that the highest optical depth at 300 GeV compatible with the VHE data (at 68% CL) is $\langle\tau_{300}\rangle \approx 3.4$, with an intrinsic index of $\alpha \approx 3.1$. Figure 4 shows how the energy dependence of pair-production absorption results in a power-law-like spectrum between 500 GeV and 10 TeV even for high optical depths, as long as the intrinsic spectrum is steep enough. This means that for an optical depth of $\langle\tau_{300}\rangle \approx 3.4$, the steep spectral index required to fit the VHE data would result in strong HE emission below 100 GeV, where pair-production absorption is no longer significant, up to a factor 100 brighter than the flux observed by *Fermi*-LAT between 10 GeV and 100 GeV. Therefore, either the

intrinsic emission from the VHE component has a sharp spectral break between 80 and 200 GeV, or the VHE instrinsic spectrum must be significantly harder than $\alpha \approx 3$. Considering the latter, and taking the *Fermi*-LAT flux between 10 GeV and 100 GeV as an upper limit to the emission of the VHE component at these energies, the optical depth should be lower than 1, as illustrated by the green model in Fig. 4. For an orbital inclination of $i = 0°$, an optical depth lower than unity indicates an emitter located farther away from the star than the compact object (at a distance of at least $\sim 3 \times 10^{12}$ cm from the compact object). At higher orbital inclinations, the limit placed on the orbit-averaged optical depth cannot be directly related to the location of the emitter, given that the optical depth would vary significantly along the orbit. However, the correlation between HE and VHE emission and the sharpness of the peak of VHE emission at superior conjunction indicate that the optical depth at this position must be low enough to not have a significant effect on the observed flux modulation, therefore excluding an emitter close to the compact object for high orbital inclinations.

Several mechanisms have been proposed to explain VHE variability and periodic modulation either by IC processes or pion production of high-energy protons with the companion wind (Kirk et al. 1999; Bosch-Ramon et al. 2006; Dermer & Böttcher 2006; Bednarek 2006; Dubus 2006; Khangulyan et al. 2008; Sierpowska-Bartosik & Torres 2008). In a leptonic scenario, the highest energy of the HESS measured spectrum can be used to derive further constraints on the location, magnetic field, and acceleration efficiency of the VHE emitter in HESS J1018−589 A. Given the energy of the stellar photons, IC scattering will take place in the deep Klein-Nishina (KN) regime, in which all of the electron energy is transferred to the scattered photons. In this scenario, the maximum energy detected (up to ∼20 TeV) would require the presence of 20 TeV electrons in the VHE emitter, which in turn requires that they are accelerated faster than their radiative energy loss timescale. The acceleration timescale can be expressed as

$$t_{\rm acc} = \eta_{\rm acc} r_{\rm L}/c \approx 0.1 \eta_{\rm acc} E_{\rm TeV} B_{\rm G}^{-1} \ {\rm s}, \quad (1)$$

where $r_{\rm L}$ is the Larmor radius of the electron, $E_{\rm TeV}$ is the electron energy in TeV units, $B_{\rm G}$ is the strength of the magnetic field in Gauss, and $\eta_{\rm acc} > 1$ is a parameter that characterizes the efficiency of the acceleration (in general $\eta_{\rm acc} \gg 1$, and only for extreme accelerators does $\eta_{\rm acc}$ approach 1, i.e. the Bohm limit). The balance between $t_{\rm acc}$ and the cooling time of electrons in the KN regime, given by $t_{\rm KN} \approx 10^3 d_{13}^2 E_{\rm TeV}^{0.7}$ s (Khangulyan et al. 2008), where d_{13} is the distance to the optical star in units of 10^{13} cm, implies $E_{\rm max} \approx (10^4 B_{\rm G} \eta_{\rm acc}^{-1} d_{13}^{-2})^{3.3}$ TeV. For IC dominant losses, and considering the maximum energy in the VHE spectrum, a minimum $B \gtrsim 2.5 \times 10^{-4} \eta_{\rm acc} d_{13}^2$ G can be derived. Furthermore, if non-radiative (adiabatic) energy losses are negligible, electron energy losses in the energy band relevant for the VHE emission would be dominated by the interplay between IC losses, which in the KN regime decrease with energy, and synchrotron losses, which increase with energy (Moderski et al. 2005). For a power-law $E_{\rm e}^{-p_{\rm inj}}$ injection spectrum with canonical $p_{\rm inj} = 2$, this results in a hardening ($p_{\rm e} \sim 1.3$) of the spectrum of the underlying steady-state particle population up to the energy for which IC and synchrotron losses are balanced, and a softening ($p_{\rm e} \sim 3$) for higher energies (see, e.g., Moderski et al. 2005; Dubus et al. 2008). The energy of the cooling break, $E_{\rm break}$, can be found from the balance of IC and synchrotron cooling timescales $t_{\rm KN} = t_{\rm syn}$, which, taking $t_{\rm syn} \approx 400 E_{\rm TeV}^{-1} B_{\rm G}^{-2}$ s, results in $E_{\rm break} \approx 0.58 (B_{\rm G} d_{13})^{-1.18}$ TeV. The relatively hard VHE spectrum detected from 1FGL J1018.6–5856 requires an evolved particle distribution with $p_{\rm e} \lesssim 2$, indicating that $E_{\rm break}$ should be higher than, or of about, the electron energies sampled by the TeV spectrum. Considering $E_{\rm break} \gtrsim 10$ TeV, the magnetic field strength is constrained by the VHE spectrum to $B \lesssim 0.1 d_{13}^{-1}$ G.

These constraints strongly depend on the location, acceleration efficiency, and magnetic field of the emission region. An extended discussion of these relationships for a VHE emitter in a binary system can be found in Khangulyan et al. (2008). For the case of 1FGL J1018.6–5856, the extension of a hard VHE spectrum up to 20 TeV indicates that acceleration/emission regions close to the compact object require an extremely efficient acceleration process, with $\eta_{\rm acc} \lesssim 50$, and magnetic field strengths between 0.001 and 0.1 G. If the emitter is located farther from the star, the constraint on the acceleration efficiency is relaxed, but the upper limit on the magnetic field is reduced to 0.03 G at $d = 3 \times 10^{13}$ cm. Regardless of the location of the emitter, the requirement that the magnetic field strength is below 0.1 G indicates that, in this scenario, the particle population responsible for the VHE emission would have a maximum 2–10 keV X-ray flux of 1.2×10^{-14} erg cm^{-2} s^{-1}, more than an order of magnitude lower than its detected X-ray flux of $(6.5 \pm 0.7) \times 10^{-13}$ erg cm^{-2} s^{-1} (Abramowski et al. 2012), a similar situation to that found for LS 5039 (Zabalza et al. 2013).

4. Conclusions

The new observations of HESS J1018–589 A with the HESS telescope array have increased the significance of the detection up to $\sim 9\sigma$, allowing the firm identification of a new VHE binary system through the measurement of its variable emission at a significance level of 4.3σ. Folding the measured flux on a 16.58-day orbit results in a phaseogram similar to the one observed at HE, with a wide peak around phase 0. The result of fitting the phaseogram to a constant flux indicates evidence of periodic flux at the 3.1σ level. The phase-averaged photon spectrum extends up to ∼20 TeV, posing constraining limits on the magnetic field ($0.001 < B < 0.1$ G). Likewise, the spectral shape above 0.350 TeV limits the γ-γ absorption and optical depth at 300 GeV to $\tau(300\,{\rm GeV}) \lesssim 1$, which will be helpful in constraining the location of the emitter once the orbital parameters are known.

Deeper observations with HESS II will improve the statistics at VHE and will provide a measurement of the spectrum below $E < 100$ GeV, allowing the investigation of key properties of the binary system such as spectral variation within the orbit or the spectral shape at low energies. Finally, the investigation of the orbital parameters through radio and optical observations is crucial to the understanding of the VHE emission mechanism in combination with the periodicity and variability observed at lower energies.

Acknowledgements. The support of the Namibian authorities and of the University of Namibia in facilitating the construction and operation of HESS is gratefully acknowledged, as is the support by the German Ministry for Education and Research (BMBF), the Max Planck Society, the German Research Foundation (DFG), the French Ministry for Research, the CNRS-IN2P3 and the Astroparticle Interdisciplinary Programme of the CNRS, the UK Science and Technology Facilities Council (STFC), the IPNP of the Charles University, the Czech Science Foundation, the Polish Ministry of Science and Higher Education, the South African Department of Science and Technology and National Research Foundation, and by the University of Namibia. We appreciate the excellent work of the technical support staff in Berlin, Durham, Hamburg, Heidelberg, Palaiseau, Paris, Saclay, and in Namibia in the construction and operation of the equipment.

References

Abdo, A. A., Ackermann, M., Ajello, M., et al. 2010, ApJS, 188, 405
Abramowski, A., Acero, F., Aharonian, F., et al. 2012, A&A, 541, A5
Acciari, V. A., Aliu, E., Arlen, T., et al. 2009, ApJ, 698, L94
Ackermann, M., Ajello, M., Ballet, J., et al. 2012, Science, 335, 189
Aharonian, F., Akhperjanian, A. G., Aye, K.-M., et al. 2005a, Science, 309, 746
Aharonian, F., Akhperjanian, A. G., Aye, K.-M., et al. 2005b, A&A, 442, 1
Aharonian, F., Akhperjanian, A. G., Bazer-Bachi, A. R., et al. 2006, A&A, 457, 899
Albert, J., Aliu, E., Anderhub, H., et al. 2006, Science, 312, 1771
Albert, J., Aliu, E., Anderhub, H., et al. 2007, ApJ, 665, L51
An, H., Dufour, F., Kaspi, V. M., & Harrison, F. A. 2013, ApJ, 775, 135
Becherini, Y., Djannati-Ataï, A., Marandon, V., Punch, M., & Pita, S. 2011, Astropart. Phys., 34, 858
Bednarek, W. 2006, MNRAS, 368, 579
Bosch-Ramon, V., Paredes, J. M., Romero, G. E., & Ribó, M. 2006, A&A, 459, L25
Böttcher, M. & Dermer, C. D. 2005, ApJ, 634, L81
Camilo, F., Bell, J. F., Manchester, R. N., et al. 2001, ApJ, 557, L51
Camilo, F., Gaensler, B. M., Gotthelf, E. V., Halpern, J. P., & Manchester, R. N. 2004, ApJ, 616, 1118
Clark, J. S., Reig, P., Goodwin, S. P., et al. 2001, A&A, 376, 476
de Naurois, M., & Rolland, L. 2009, Astropart. Phys., 32, 231
Dermer, C. D., & Böttcher, M. 2006, ApJ, 643, 1081
Dubus, G. 2006, A&A, 451, 9
Dubus, G., Cerutti, B., & Henri, G. 2008, A&A, 477, 691
Hadasch, D., Torres, D. F., Tanaka, T., et al. 2012, ApJ, 749, 54
Hoffmann, A. D., Klochkov, D., Santangelo, A., et al. 2009, A&A, 494, L37
Khangulyan, D., Aharonian, F., & Bosch-Ramon, V. 2008, MNRAS, 383, 467
Kirk, J. G., Ball, L., & Skjæraasen, O. 1999, Astropart. Phys., 10, 31
Li, J., Torres, D. F., Chen, Y., et al. 2011, ApJ, 738, L31
Milne, D. K., Caswell, J. L., Kesteven, M. J., Haynes, R. F., & Roger, R. S. 1989, Proc. Astron. Soc. Austr., 8, 187
Moderski, R., Sikora, M., Coppi, P. S., & Aharonian, F. 2005, MNRAS, 363, 954
Moskalenko, I. V., & Karakula, S. 1994, ApJS, 92, 567
Pavlov, G. G., Misanovic, Z., Kargaltsev, O., & Garmire, G. P. 2011, ATel, 3228
Piron, F., Djannati-Atai, A., Punch, M., et al. 2001, A&A, 374, 895
Scargle, J. D. 1982, ApJ, 263, 835
Sierpowska-Bartosik, A., & Torres, D. F. 2008, Astropart. Phys., 30, 239
Takahashi, T., Kishishita, T., Uchiyama, Y., et al. 2009, ApJ, 697, 592
Zabalza, V., Bosch-Ramon, V., Aharonian, F., & Khangulyan, D. 2013, A&A, 551, A17

[1] Universität Hamburg, Institut für Experimentalphysik, Luruper Chaussee 149, 22761 Hamburg, Germany
[2] Max-Planck-Institut für Kernphysik, PO Box 103980, 69029 Heidelberg, Germany
[3] Dublin Institute for Advanced Studies, 31 Fitzwilliam Place, Dublin 2, Ireland
[4] National Academy of Sciences of the Republic of Armenia, Marshall Baghramian Avenue, 24, 0019 Yerevan, Armenia
[5] Yerevan Physics Institute, 2 Alikhanian Brothers St., 375036 Yerevan, Armenia
[6] Institut für Physik, Humboldt-Universität zu Berlin, Newtonstr. 15, 12489 Berlin, Germany
[7] University of Namibia, Department of Physics, Private Bag 13301, Windhoek, Namibia
[8] GRAPPA, Anton Pannekoek Institute for Astronomy, University of Amsterdam, Science Park 904, 1098 XH Amsterdam, The Netherlands
[9] Department of Physics and Electrical Engineering, Linnaeus University, 351 95 Växjö, Sweden
[10] Institut für Theoretische Physik, Lehrstuhl IV: Weltraum und Astrophysik, Ruhr-Universität Bochum, 44780 Bochum, Germany
[11] GRAPPA, Anton Pannekoek Institute for Astronomy and Institute of High-Energy Physics, University of Amsterdam, Science Park 904, 1098 XH Amsterdam, The Netherlands
[12] Institut für Astro- und Teilchenphysik, Leopold-Franzens-Universität Innsbruck, 6020 Innsbruck, Austria
[13] School of Chemistry & Physics, University of Adelaide, 5005 Adelaide, Australia
[14] Centre for Space Research, North-West University, 2520 Potchefstroom, South Africa
[15] LUTH, Observatoire de Paris, CNRS, Université Paris Diderot, 5 place Jules Janssen, 92190 Meudon, France
[16] LPNHE, Université Pierre et Marie Curie Paris 6, Université Denis Diderot Paris 7, CNRS/IN2P3, 4 place Jussieu, 75252 Paris Cedex 5, France
[17] Laboratoire Univers et Particules de Montpellier, Université Montpellier 2, CNRS/IN2P3, CC 72, place Eugène Bataillon, 34095 Montpellier Cedex 5, France
[18] DSM/Irfu, CEA Saclay, 91191 Gif-Sur-Yvette Cedex, France
[19] Astronomical Observatory, The University of Warsaw, Al. Ujazdowskie 4, 00-478 Warsaw, Poland
[20] Aix-Marseille Université, CNRS/IN2P3, CPPM UMR 7346, 13288 Marseille, France
[21] Instytut Fizyki Jądrowej PAN, ul. Radzikowskiego 152, 31-342 Kraków, Poland
[22] Funded by EU FP7 Marie Curie, grant agreement No. PIEF-GA-2012-332350,
[23] School of Physics, University of the Witwatersrand, 1 Jan Smuts Avenue, Braamfontein, 2050 Johannesburg, South Africa
[24] Landessternwarte, Universität Heidelberg, Königstuhl, 69117 Heidelberg, Germany
[25] Oskar Klein Centre, Department of Physics, Stockholm University, Albanova University Center, 10691 Stockholm, Sweden
[26] Institut für Astronomie und Astrophysik, Universität Tübingen, Sand 1, 72076 Tübingen, Germany
[27] Laboratoire Leprince-Ringuet, École Polytechnique, CNRS/IN2P3, 91128 Palaiseau, France
[28] APC, AstroParticule et Cosmologie, Université Paris Diderot, CNRS/IN2P3, CEA/Irfu, Observatoire de Paris, Sorbonne Paris Cité, 10 rue Alice Domon et Léonie Duquet, 75205 Paris Cedex 13, France
[29] Univ. Grenoble Alpes, IPAG, 38000 Grenoble, France
CNRS, IPAG, 38000 Grenoble, France
[30] Department of Physics and Astronomy, The University of Leicester, University Road, Leicester, LE1 7RH, UK
[31] Nicolaus Copernicus Astronomical Center, ul. Bartycka 18, 00-716 Warsaw, Poland
[32] Institut für Physik und Astronomie, Universität Potsdam, Karl-Liebknecht-Strasse 24/25, 14476 Potsdam, Germany
[33] Laboratoire d'Annecy-le-Vieux de Physique des Particules, Université Savoie Mont-Blanc, CNRS/IN2P3, 74941 Annecy-le-Vieux, France
[34] DESY, 15738 Zeuthen, Germany
[35] Obserwatorium Astronomiczne, Uniwersytet Jagielloński, ul. Orla 171, 30-244 Kraków, Poland
[36] Université Bordeaux, CNRS/IN2P3, Centre d'Études Nucléaires de Bordeaux Gradignan, 33175 Gradignan, France
[37] Universität Erlangen-Nürnberg, Physikalisches Institut, Erwin-Rommel-Str. 1, 91058 Erlangen, Germany
[38] Centre for Astronomy, Faculty of Physics, Astronomy and Informatics, Nicolaus Copernicus University, Grudziadzka 5, 87-100 Torun, Poland
[39] Department of Physics, University of the Free State, PO Box 339, Bloemfontein 9300, South Africa
[40] Heisenberg Fellow (DFG), ITA Universität Heidelberg, Germany
[41] GRAPPA, Institute of High-Energy Physics, University of Amsterdam, Science Park 904, 1098 XH Amsterdam, The Netherlands
[42] Now at Institut de Ciències de l'Espai (IEEC-CSIC), Campus UAB, Fac. de Ciències, Torre C5, parell, 2a planta, 08193 Barcelona, Spain